Journal of Volcanology and Geothermal Research 278–279 (2014) 96–102

Contents lists available at ScienceDirect

Journal of Volcanology and Geothermal Research

journal homepage: www.elsevier.com/locate/jvolgeores

Ground deformation associated with the eruption of Lumpur Sidoarjo mud volcano, east Java, Indonesia

Yosuke Aoki *, Teguh Purnama Sidiq [1]

Earthquake Research Institute, University of Tokyo, 1-1 Yayoi 1, Bunkyo-ku, Tokyo 113-0032, Japan

ARTICLE INFO

Article history:
Received 17 July 2013
Accepted 14 April 2014
Available online 25 April 2014

Keywords:
Mud volcano
Ground deformation
Synthetic aperture radar
Time-series analysis

ABSTRACT

Ground deformation associated with the eruption of Lumpur Sidoarjo mud volcano between 2006 and 2011 has been investigated from Synthetic Aperture Radar images. Marked subsidence has been observed to the west of, as well as around, the vent. Line-of-sight changes in the both areas decayed since the middle of 2008 with a time constant of 1.5–2.5 years, implying that the ongoing eruption won't last long. This uniform decay time indicates that the western part is connected to the eruption center since the middle of 2008 to form a system with stationary geometry. Our observation that the decay started later to the west than around the vent suggests that the subsidence to the west has been triggered by the mud eruption. A simple modeling suggests that 1) the conduit needs to be narrower at depth than at the surface, 2) the effective rigidity of the mud needs to be lower than that estimated from the drilled sample, or both to explain the observed decay constant of the deformation.

1. Introduction

Mud volcanism is a process that drives materials in the sediment to the surface. It shares common features with magmatic volcanism. For example, both of them often form calderas and aligned vents that are controlled by ambient stress (e.g., Bonini, 2012). Nevertheless, the mechanics of mud volcanism is not as well studied as that of magmatic volcanism because of its rare occurrence. With this background, the eruption of Lumpur Sidoarjo (LUSI), eastern Java Island, Indonesia, provides us with a precious opportunity to observe the mud volcanism from its birth.

LUSI, which has been erupting since 29 May 2006, is located in the eastern Java Island, a region prone to mud volcanism due to an extensive sedimentation (Fig. 1a; Mazzini et al., 2007, 2009). Fig. 2 summarizes the evolution of mud extrusion rates taken from published literatures. The extrusion rate was around 50,000 m^3/day during the first few months (Istadi et al., 2009). It increased to 125,000 m^3/day in September 2006, four months after the onset and reached its maximum of 180,000 m^3/day (Mazzini et al., 2007, 2009; Istadi et al., 2009) before decreasing to 90,000 m^3/day in August 2008 and less than 10,000 m^3/day by the middle of 2010 (Mazzini et al., 2009; Rudolph et al., 2013). The extruded mud buried more than an area of 7 km^2, forced more than 60,000 people to evacuate, and caused more than 4 billion US dollars of damage (e.g., Rudolph et al., 2013).

With this background, it is important to understand the mechanics of the LUSI eruption and an eruption of mud volcano in general. From a practical point of view, it is important to evaluate the longevity of the eruption. Some previous studies estimated the longevity of tens of years from physical modeling (Istadi et al., 2009; Davies et al., 2011; Rudolph et al., 2011). Rudolph et al. (2013) challenged the previous studies with Synthetic Aperture Radar (SAR) data to conclude that the eruption will decay in a few years because the deformation has been decaying with a characteristic time of a few years.

Here we follow a similar path with Rudolph et al. (2013) to derive the evolution of the displacement field associated with the LUSI eruption from SAR images taken from the ALOS satellite (Shimada et al., 2008), which yields good coherence even in vegetated regions like Indonesia. While Rudolph et al. (2013) used SAR images only from the descending orbit, we used images from the ascending orbit as well to gain more insights into the evolution of the deformation. Our main finding is that the deformation associated with the mud eruption extends to the west as well as around the vent. This suggests that the mud is fed from the west of the vent where a gas field extends, as well as from right beneath the vent.

2. SAR images and processing

We processed a total of 93 SAR images from five different paths, two of which are from the ascending orbit and three are from the descending orbit (Fig. 1b, Table 1). Images from some paths have spans of more than four years, much of the lifetime of the ALOS satellite, while some span only about a year (Table 1).

We processed the SAR data by the StaMPS software (Hooper, 2008) to derive the temporal evolution of persistent scatterers. Fig. 3 shows

* Corresponding author. Tel.: +81 3 5841 8283; fax: +81 3 3812 6979.
E-mail addresses: yaoki@eri.u-tokyo.ac.jp (Y. Aoki), teguh.purnama@yahoo.com (T.P. Sidiq).
[1] Now at Geodesy Research Group, Institute of Technology Bandung, Jl. Ganesha 10, Bandung 40132, Indonesia.

http://dx.doi.org/10.1016/j.jvolgeores.2014.04.012
0377-0273/

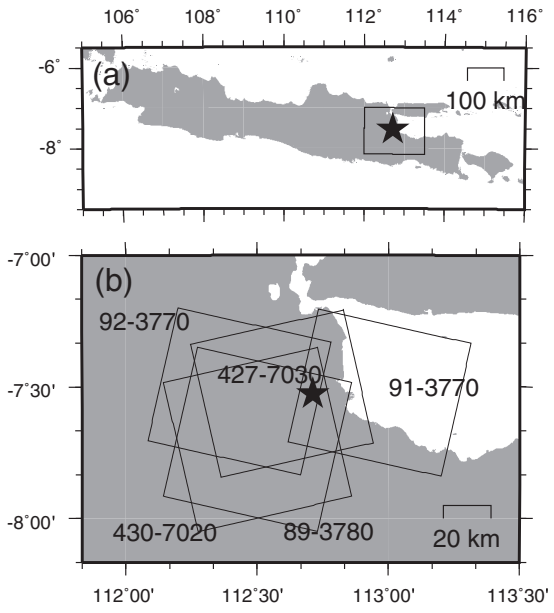

Fig. 1. (a) Location of LUSI mud volcano shown by star. Rectangle depicts the area shown in (b). (b) A close-up map around LUSI shown by star. Rectangles represent the spatial extent of SAR images used in this study. Paths and frames of the SAR images are also shown.

the spatial distribution of total line-of-sight (LOS) changes during the observation period obtained by images from each track. Images from 89–3780 give much smaller total LOS changes (Fig. 3e) because the images from this track spans only about a year. Total displacements from other four tracks (Fig. 3a–d) give similar spatial pattern, with a maximum LOS extension of about 200 mm. A similar pattern between ascending and descending images, which have roughly an opposite sensitivity to east–west displacements, suggests that the observed LOS extension is dominated by subsidence rather than horizontal displacements. The actual maximum LOS extension around the vent is probably larger than the observation because the mud extrusion prevents us from obtaining coherent interferograms close to the vent. Note that the method we employed in this study gives the time series of persistent scatterers only when they are coherent during the whole time period (Hooper, 2008) so that the time series near the vent cannot be obtained because of the decoherence due to mud extrusion. This leads to poorer data coverage near the vent than previous studies (Fukushima et al., 2009; Rudolph et al., 2013). Fig. 3 also shows that the area of LOS extension is not limited around the vent, shown by star, but extended to the west, where the Wanut gas field exists.

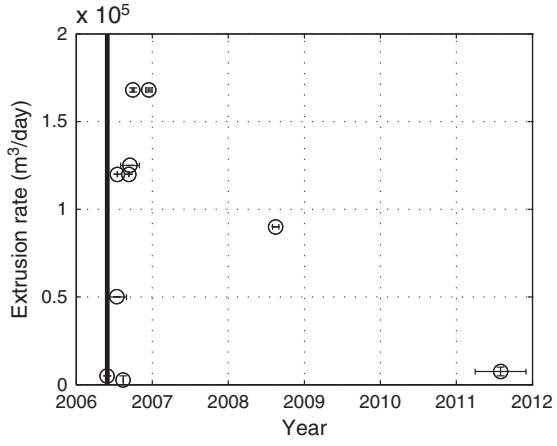

Fig. 2. Temporal evolution of the mud extrusion rate taken from published literatures (Mazzini et al., 2007, 2009, 2012; Istadi et al., 2009). Lengths of error bars, in particular for the extrusion rate, are somewhat arbitrary. The vertical bar indicates the time of the onset of the eruption.

While LOS extension is prevailing in most of the area from both ascending and descending images, an exception is seen to the northwest of the vent, where LOS contraction and extension are observed from ascending and descending images, respectively (Fig. 3). This pattern indicates a dominance of westward motion there and the observed deformation is not due to the mud extrusion but due to something else, possibly due to a faulting (Mazzini et al., 2007). Here we do not explore the cause of the deformation observed to the northeast of the vent.

Because of the mud extrusion and accumulation on the surface, it is also possible that the observed LOS extension is due to the elastic response of the Earth by the mud loading. Here we exploit this possibility by simply assuming a point loading of mud with a mass $M = \rho_e V_e$ where ρ_e and V_e are density and volume of the extruded mud as done by Fukushima et al. (2009) who concluded that the deformation caused by mud loading is negligible. Here we test whether we can still ignore the effect of mud loading to explain the deformation field between 2006 and 2011, instead of the first five months of the eruption tested by Fukushima et al. (2009). Note that he extruded mud volume between 2006 and 2011 is about 10 times larger than that during the first five months.

This problem is known as the Boussinesq problem (Boussinesq, 1878; Jaeger et al., 2007, pp. 408), in which the radial and vertical displacements, u_r and u_z, respectively, are given as a function of radial distance r by

$$u_r = \frac{(1+\nu)(1-2\nu)}{4\pi E_c}\frac{Mg}{r}, \tag{1}$$

$$u_z = -\frac{1-\nu^2}{2\pi E_c}\frac{Mg}{r} \tag{2}$$

where E_c and ν represent Young's modulus and Poisson's ratio of the crust, respectively, and g denotes gravitational acceleration.

Assuming $E_c = 5$ GPa, $\nu = 0.25$ and $\rho_e = 1500\ kg/m^3$ obtained from drilling samples (Istadi et al., 2009) and $V_e = 7\times10^7\ m^3$ from the buried area of ~7 km^2 and the average mud height of ~10 m, the displacement at $r = 2\ km$ is $u_r = 4.7\ mm$ and $u_z = 14.0\ mm$. This corresponds to the LOS extension of at most ~14 mm, which is larger than the detection threshold but much smaller than the observed LOS extension of up to ~200 mm. We can thus safely conclude that the mud loading contributes less than 10% of the observed LOS changes, although it is not completely negligible. Note that there is no mud loading to the west of the vent where significant LOS extension was observed so that the LOS extension is purely due to the depressurization at depth.

3. Evolution of displacements

Next we explored the evolution of LOS changes at representative points shown in Fig. 3. The obtained time series, particularly for western points (Fig. 4a,b), shows accelerations in the LOS displacements until early to middle of 2008, or 1.5 to 2 years after the onset of the eruption, before subsequent deceleration.

We then tried to fit each time series in $t_0 > 2008.408\ yr$, or more than two years from the eruption onset, by exponential functions as

$$d = Aexp\left(-\frac{t}{\tau}\right) + C \tag{3}$$

where d is the observed LOS changes and t is time. A, C, and τ are model parameters to be estimated to minimize the sum of squared residuals. Here τ is called the relaxation time where the displacement rate decays by $1/e$ in τ years.

Table 1
List of SAR images used in this study.

Path–frame	LOS direction[a]	Start date	End date	Span (yr)	# of images
89–3780	[−0.719, 0.154, −0.678]	3 Jan. 2007	21 Feb. 2008	1.13	9
91–3770	[−0.611, 0.131, −0.780]	24 Mar. 2007	4 Apr. 2011	4.30	22
92–3770	[−0.611, 0.131, −0.780]	8 Oct. 2006	21 Apr. 2011	4.53	25
427–7030	[0.611, 0.131, −0.780]	30 Dec. 2006	25 Feb. 2011	4.16	21
430–7020	[0.719, 0.154, −0.678]	19 May 2006	9 Jan. 2009	2.62	14

[a] Unit vectors of LOS. The first, second, and third components correspond to the east, north, and vertical components, respectively.

The derived relaxation times do not vary much between western and eastern points; they are mostly between 1.5 and 2.5 years (Fig. 4). Note that a relaxation time is estimated only when an *F*-test (e.g., Menke, 2012, pp. 111–112) shows that an exponential curve fits the time series better than a linear fit with a confidence of 95%. Thus a relaxation time is not obtained from noisy or short time series. (Fig. 4).

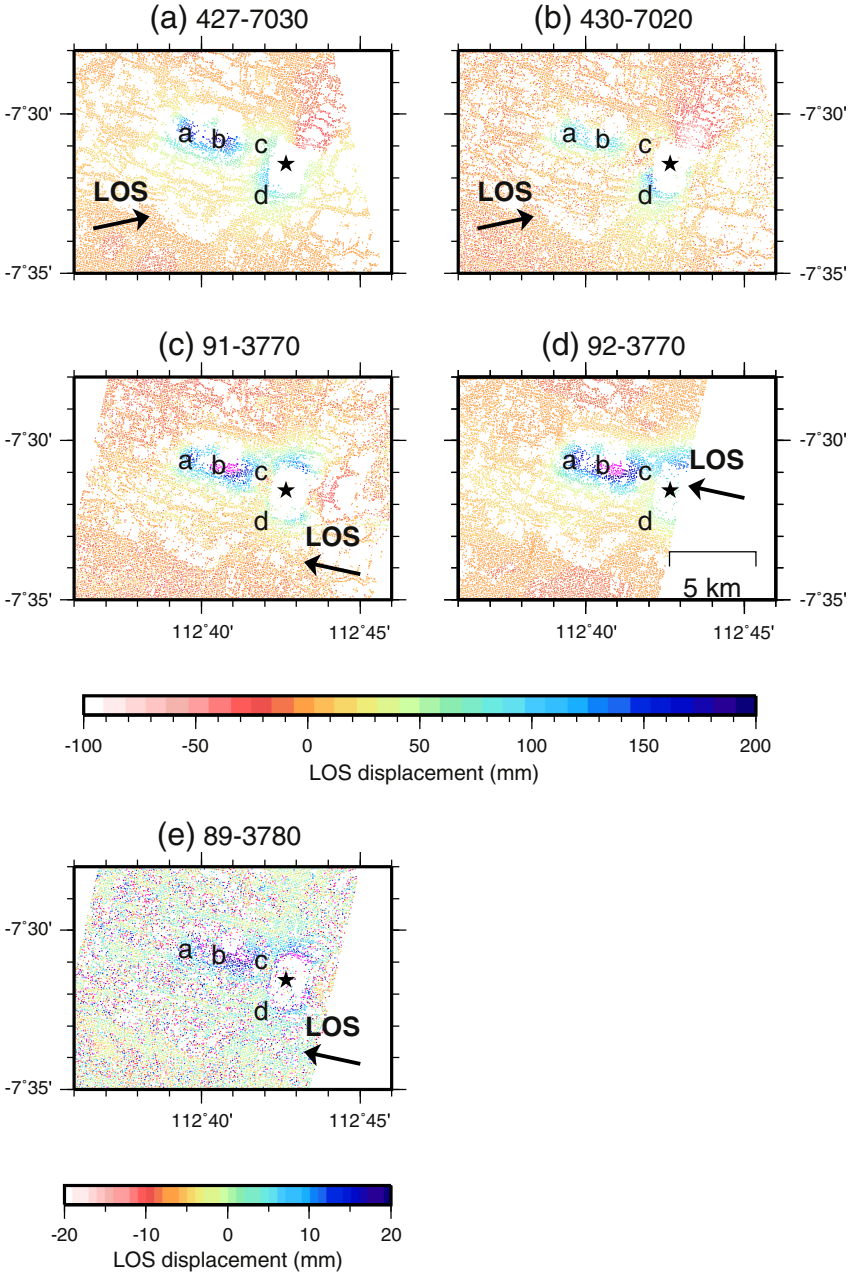

Fig. 3. Total LOS displacements derived from SAR images for each path. Note that subsidence leads to a positive LOS displacement. Star depicts the location of the vent. The horizontal projection of the LOS vectors is also shown. Characters a, b, c, and d depict points where temporal evolution is plotted in Fig. 4. SAR images from 89–3780 (e) have shorter time span (Table 1) so that the total LOS change is smaller. Because of this, a different color scale is employed. Note that incoherence of SAR images due to the mud extrusion prevents us to obtain LOS changes close to the vent.

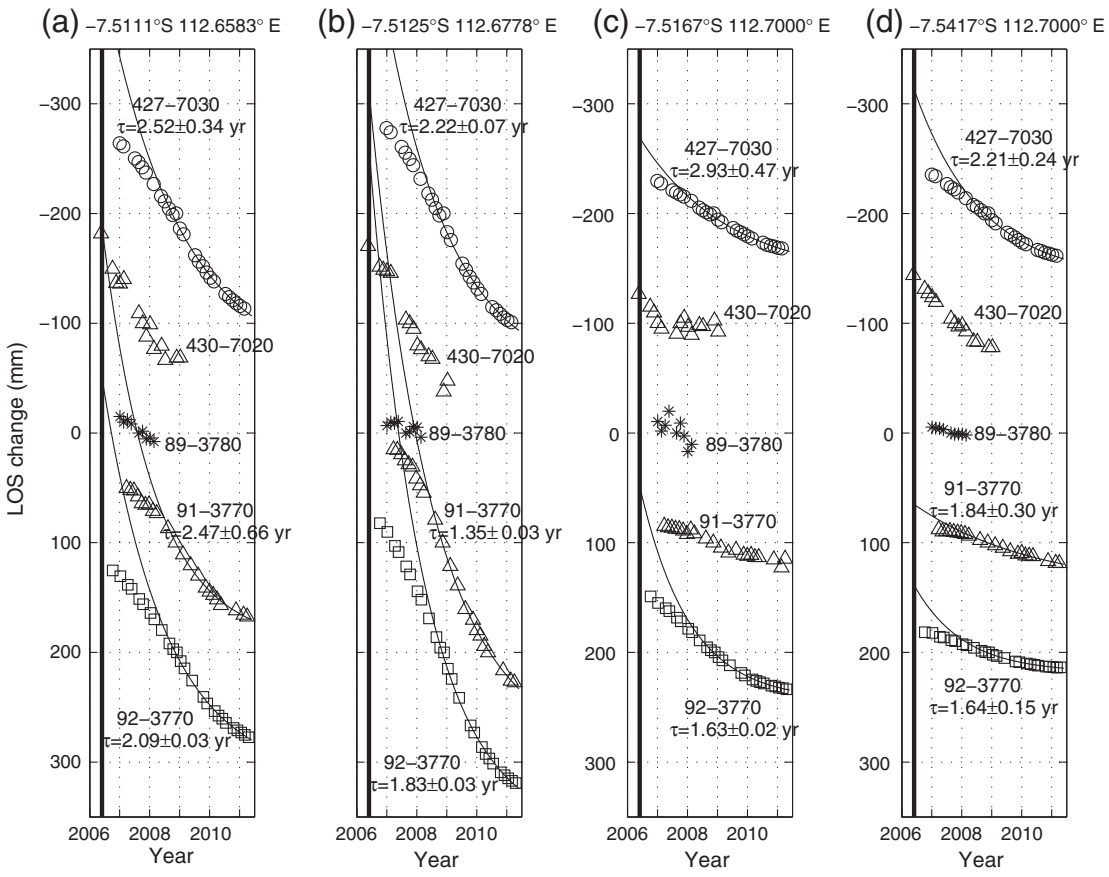

Fig. 4. Temporal evolution of LOS changes for four representative points whose location is shown in Fig. 3. Solid curves denote the calculated LOS changes by exponential curves (Eq. (3)) to fit the observed LOS changes more than two years after the onset of the eruption (t > 2008.408). They are shown only when an *F*-test (Menke, 2012, p. 111–112) gives a better fit with an exponential fit than a straight-line regression by a confidence level of 95%.

4. Discussion

4.1. Insights from the observation

As long as an elastic medium is assumed, the relaxation time of around 2 years suggests that the depressurization at depth is also decelerating with a time constant of around 2 years. Because the evolution of depressurization is viewed as a good proxy for that of mud extrusion, our result indicates that the mud eruption will cease soon, contrary to earlier studies (Istadi et al., 2009; Davies et al., 2011; Rudolph et al., 2011) that forecasted that the eruption will likely last for decades. This rapid decay of deformation is qualitatively consistent with the mud extrusion rate that decayed to 5000–10,000 m^3/day in 2011 from its maximum of ~180,000 m^3/day and ~90,000 m^3/day in August 2008 (Istadi et al., 2009; Mazzini et al., 2012, Fig. 2).

Fig. 4 shows that the departure from the exponential decay before mid-2008 is bigger in the western points than those in the east. This reflects an earlier onset of the exponential decay to the east. While Rudolph et al. (2013) derived a longer decay time to the west, their estimate is probably biased by the delayed onset of the exponential decay to the west. Combining our results with an observation that the deformation to the west is subtle, if not null, during the first six months of the eruption, in contrast with a significant deformation around the vent (Fukushima et al., 2009), we conclude that the deformation to the west was triggered by the eruption with some delay, accelerated, and then started to decay later than that around the vent. This temporal evolution suggests that the western subsidence could be connected to the near-vent subsidence. Give that the area of western subsidence corresponds to a gas field, however, it is also possible to interpret that the western subsidence does not have anything to do with the mud eruption but due to a gas extraction. To confirm the cause of the subsidence, we need independent information such a time series of the amount of gas extraction there.

4.2. A simple physical model

Here we consider a simple model to constrain the geometry of the mud volcano system that is consistent with the decay constant of the observed LOS changes after the middle of 2008. See Table 2 for symbols and descriptions of parameters used in this study. Following Zoporowski and Miller (2009), let us assume a situation in which mud with density ρ_c ascends by velocity v from a cylindrical reservoir of volume V_r at depth h connected to a cylindrical conduit with cross-sectional area A leading vertically to the surface (Fig. 5).

Conservation of mass and momentum in the one-dimensional conduit is given by

$$\frac{d\rho_c}{dt} + \frac{d(\rho_c v)}{dz} = 0 \tag{4}$$

where z is the vertical direction with positive upwards and t represents time. If we assume an isochronic flow in the conduit, ρ_c and v are independent of position z, so that Eq. (4) leads to

$$\frac{d\rho_c}{dt} = 0. \tag{5}$$

Table 2
Parameter symbols and descriptions used in this study.

Symbol	Definition (unit)	Typical value
A	Cross-sectional area of the conduit (m^2)	$6^{a,b} - \times 10^{3c}$
a	Radius of the mud chamber (m)	1000^{d}
d	Observed LOS change (m)	
η	Mud viscosity (Pa · s)	10^{4e}
g	Gravitational acceleration (m/s^2)	9.81
Γ	Compliance of the mud reservoir (m^3/Pa)^{f}	
h	Height of the conduit (m)	$1500^{d,g}$
I	Flux of mud into the mud reservoir (m^3/s)	
μc	Rigidity of the crust (GPa)	2^{b}
μm	Rigidity of mud in the conduit (GPa)	2^{g}
ν	Poisson's ratio	0.25
p	Pressure at the mud reservoir (Pa)	
Q	Mud discharge rate (m^3/s)	
ρc	Mud density in the conduit (kg/m^3)	1500^{g}
ρe	Density of the extruded mud (kg/m^3)	1500^{g}
τ	Time constant for exponential relaxation (1/s)	
uz	Vertical displacement (m)	
ur	Radial displacement (m)	
Ve	Volume of the extruded mud (m^3)	7×10^7
Vr	Volume of the mud reservoir (m^3)	10^7
v	Velocity of ascending mud	
β	Compressibility of the mud (1/Pa)^{h,i}	3×10^{-10}
E	Young's modulus of the crust (GPa)^{j}	5

a: The value taken in a numerical simulation by Rudolph et al. (2011).
b: Our study suggests a lower value.
c: Visual inspection of the current vent.
d: Depth of the mud reservoir inferred from InSAR observations by Fukushima et al. (2009).
e: The value taken in a numerical simulation by Rudolph et al. (2011) based on sample measurements (Mazzini et al., 2007; Manga et al., 2009; Rudolph and Manga (2010)).
f: The value depends on the shape of the mud reservoir.
g: Depth of the mud source estimated from the P-wave velocity and density of mud samples (Istadi et al., 2009).
h: Derived from given μm and ν by $\beta = 3(1 - 2\nu) / (2\,\mu m(1 + \nu))$.
i: Our study suggests a higher value.
j: Derived from given μm and ν by $E = 2\mu c(1 + \nu)$.

Conservation of momentum is described by the one-dimensional Navier–Stokes equation with negligible convection as

$$\frac{d(\rho_c v)}{dt} = -\frac{dp}{dz} - \rho_c g - \frac{8\pi\eta v}{A} \tag{6}$$

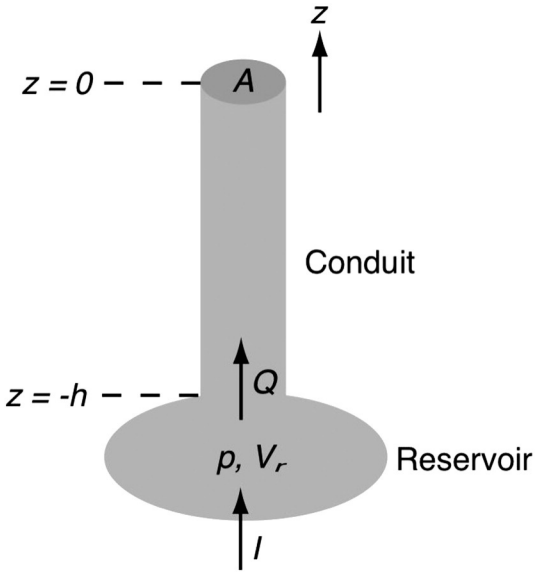

Fig. 5. A conceptional model of the mud volcano model.

where η and g denote constant dynamic viscosity and gravitational acceleration, respectively. Here we took a constant viscosity of 10^4 Pa·s, the value taken in from a numerical simulation by Rudolph et al. (2011) based on sample measurements (Mazzini et al., 2007; Manga et al., 2009; Rudolph and Manga, 2010). This value is comparable with that of mafic magmas, but we assumed a depth-independent viscosity unlike that in the modeling of magmatic eruptions. While the viscosity increase by vesiculation makes a significant role in conduit processes during magmatic eruptions (e.g., Gonnermann and Manga, 2007), we can assume a constant viscosity in this case because the presence of stable gas hydrates on mud breccia provides little opportunity for degassing (Murton and Biggs, 2003).

Combining Eqs. (5) and (6) and replacing $-dp/dz$ with p/h gives a differential equation with respect to flux $Q = Av$ as

$$\frac{dQ}{dt} = -\frac{8\pi\eta}{\rho_c A}Q + \frac{A}{\rho_c h}p - Ag. \tag{7}$$

Conservation of the fluid mass inside the reservoir is described as

$$\frac{d(\rho_c V_r)}{dt} = \rho_c(I - Q) \tag{8}$$

where I denotes the influx of mud. Eq. (8) is rewritten using mud compressibility β

$$\beta = \frac{1}{\rho_c}\frac{d\rho_c}{dp} \tag{9}$$

as

$$\frac{dp}{dt} = \frac{1}{\beta V_r}\left(I - Q - \frac{dV_r}{dt}\right). \tag{10}$$

V_r and p are related by

$$dV_r = \Gamma dp \tag{11}$$

where Γ is compliance of the reservoir which depends on the shape of the mud reservoir. For example,

$$\Gamma = \frac{8(1-\nu)a^3}{3\mu_c} \tag{12}$$

for a horizontal circular sill with radius a embedded in a homogeneous, elastic, and isotropic halfspace with rigidity μ_c (Fialko et al., 2001). Eq. (12) is derived with an approximation that the depth of the sill is larger than its radius. Combining Eqs. (10) and (11) gives

$$\frac{dp}{dt} = \frac{I - Q}{\beta V_r + \Gamma}. \tag{13}$$

Eqs. (7) and (13) form a simultaneous differential equation described in matrix form as

$$\frac{d}{dt}\begin{bmatrix} p \\ Q \end{bmatrix} = \boldsymbol{R}\begin{bmatrix} p \\ Q \end{bmatrix} + \begin{bmatrix} I/(\beta V_r + \Gamma) \\ -Ag \end{bmatrix}, \tag{14}$$

$$\boldsymbol{R} = \begin{bmatrix} 0 & -1/(\beta V_r + \Gamma) \\ A/(\rho_c h) & -8\pi\eta/(\rho_c A) \end{bmatrix}. \tag{15}$$

Solving this equation, the mud chamber pressure p, the change of which results in observed LOS changes in this case, is written as

$$p(t) = c_1 e^{\lambda_+ t} + c_2 e^{\lambda_- t} + p(\infty) \tag{16}$$

$$Q(t) = c_3 e^{\lambda_+ t} + c_4 e^{\lambda_- t} + Q(\infty) \tag{17}$$

where c_1, c_2, c_3, and c_4 are constants derived by solving Eqs. (14) and (15), and λ_+ and λ_- correspond to eigenvalues of $\boldsymbol{R}$ that are

$$\lambda_\pm = -\frac{4\pi\eta}{\rho_c A}\left(1 \pm \sqrt{1 - \frac{A^2}{4\pi h\eta(\beta V_r + \Gamma)}}\right) \tag{18}$$

and

$$\begin{bmatrix} p(\infty) \\ Q(\infty) \end{bmatrix} = \boldsymbol{R}^{-1}\begin{bmatrix} -I/(\beta V_r + \Gamma) \\ Ag \end{bmatrix} = \frac{A}{\rho_c h(\beta V_r + \Gamma)}\begin{bmatrix} 8\pi\eta I/(\rho_c h) + Ag \\ AI/(\rho_c h) \end{bmatrix}. \tag{19}$$

If $A^2 > 4\pi h\eta(\beta V_r + \Gamma)$, in which the system is underdamped, the temporal evolution of p is represented by an oscillation with amplitude decaying exponentially. In this case, The amplitude decay has a time constant of $rho_c A/(4\pi\eta)$. If $A^2 < 4\pi h\eta(\beta V_r + \Gamma)$, on the other hand, the system is overdamped and the temporal evolution of p is described by exponential decays with two time constants, $-1/\lambda_+$ and $-1/\lambda_-$.

Here we examine whether the system of LUSI is over or underdamped by applying realistic values (Table 2). If the system were underdamped, the characteristic decay time is $\rho_c A/(4\pi\eta)$ (Eq. 18). Assuming realistic parameters (see Eq. (12) and Table 2) requires $A > 1.4 \times 10^4\ m^2$, indicating that the radius of the conduit needs to be large than ~66 m for the system to be underdamped. This value is larger than the radius of the current vent that is at most 35 m and the effective radius suggested by Rudolph et al. (2011) from numerical simulations (1 m). Thus the system should be highly overdamped with $A^2 \ll 4\pi h\eta(\beta V + \Gamma)$. Eq. (18) can then be rewritten by

$$\lambda_+ = -\frac{8\pi\eta}{\rho_c A}\left(1 - \frac{A^2}{16\pi h\eta(\beta V_r + \Gamma)}\right) \tag{20}$$

$$\lambda_- = \frac{-A}{2\rho_c h(\beta V_r + \Gamma)} \tag{21}$$

where λ_+ and λ_- correspond to the shorter and longer relaxation time, respectively. Surprisingly, Eq. (21) indicates that the longer relaxation time does not depend on the dynamic viscosity of mud η.

Here we explore possible parameter sets to be consistent with the observation that has a relaxation time of about 2 years or $\lambda_- = 1.58 \times 10^{-8}$/s. Substituting a value taken from a numerical simulation by Rudolph et al. (2011) ($A = 6\ m^2$; Table 2) gives $\lambda_- \sim 1.33 \times 10^{-6}$/s or a relaxation time of about 8.7 days, two orders of magnitude shorter than the observation. Eq. (21) suggests smaller A, smaller μ_m, larger a, larger V_r or a combination of these are required to be consistent with the observation. Given the spatial extent of the observed LOS displacements, a and V_r may not be much larger than those currently assigned. Smaller A, smaller μ_m, or both are thus required to match up with the observation. For example, $\mu_m = 0.2$ GPa and $A = 0.6\ m^2$, both of which are an order of magnitude smaller than the previous values, give $\lambda_- \sim 1.33 \times 10^{-8}$/s or a relaxation time of ~2.4 years, more consistent with the observation. Although Istadi et al. (2009) derived the rigidity of the mud as ~2 GPa from drilling samples, it might not represent the rigidity of the mud responsible for the eruption but represent the bulk property around the mud volcano. While visual inspection from satellite images suggests that the conduit has a diameter of about 70 m or $A \sim 4 \times 10^3\ m^2$ at the surface, the conduit is probably, at least effectively, narrower at depth.

5. Conclusion

We derived the temporal evolution of ground deformation associated with the eruption of LUSI mud volcano between 2006 and 2011 from a time series analysis of SAR images from the ALOS satellite. Our results show that the marked subsidence is observed to the west of the eruption center as well as around the vent. The observed total LOS changes are up to 200 mm or more. We also inferred that the LOS changes decays exponentially after the middle of 2008 with a time constant of 1.5–2.5 years in the both areas. This short decay time indicates that the eruption won't last long. This observation also shows that the near-vent area and western part have been connected since the middle of 2008 with a stationary geometry. The creation of this system makes the mud extrusion controlled by a pressure gradient between the mud reservoir and surface. The time series we obtained also revealed that the onset of the exponential decay around the vent is earlier than the western part by about a half year. We also observed that the subsidence in the western part has been accelerated until 2007 when the subsidence around the vent had stopped accelerating. These observations suggest that the subsidence to the west has been triggered by the mud eruption with time delay.

Acknowledgments

PALSAR level 1.0 data from the ALOS satellite are shared among PIXEL (PALSAR Interferometry Consortium to Study our Evolving Land surface), and provided by the Japan Aerospace Exploration Agency (JAXA) under a cooperative research contract with the Earthquake Research Institute, University of Tokyo. The ownership of PALSAR data belongs to the Ministry of Economy, Trade, and Industry, and JAXA. Some figures are created with the Generic Mapping Tools [Wessel and Smith, 1998]. Reviews by three anonymous referees improved the manuscript.

References

Bonini, M., 2012. Mud volcanoes: indicators of stress orientation and tectonic controls. Earth-Sci. Rev. 115, 121–152. http://dx.doi.org/10.1016/j.earscirev.2012.09.002.
Boussinesq, J., 1878. Équilibre élastique d'un solide isotrope de masse négligeable, soumis à différents poids. CR Acad. Sci. Paris 86, 1260–1263.
Davies, R.J., Mathias, S.A., Swarbrick, R.E., Tingay, M.J., 2011. Probabilistic longevity estimate for the LUSI mud volcano, East Java. J. Geol. Soc. 168, 517–523. http://dx.doi.org/10.1144/0016-76492010-129.
Fialko, Y., Khazan, Y., Simons, S., 2001. Deformation due to a pressurized horizontal circular crack in an elastic half-space, with applications to volcano geodesy. Geophys. J. Int. 146, 181–190. http://dx.doi.org/10.1046/j.1365-246X.2001.00452.x.
Fukushima, Y., Mori, J., Hashimoto, M., Kano, Y., 2009. Subsidence associated with the LUSI mud eruption, East Java, investigated by SAR interferometry. Mar. Pet. Geol. 26, 1740–1750. http://dx.doi.org/10.1016/j.marpetgeo.2009.02.001.
Gonnermann, H., Manga, M., 2007. The fluid mechanics inside a volcano. Annu. Rev. Fluid Mech. 39, 321–356. http://dx.doi.org/10.1146/annurev.fluid.39.050905.110207.
Hooper, A., 2008. A multi-temporal InSAR method incorporating both persistent scatterer and small baseline approaches. Geophys. Res. Lett. 35. http://dx.doi.org/10.1029/2008GL03465 (L16302).
Istadi, B.P., Pramono, G.H., Sumintadireja, P., Alam, S., 2009. Modeling study of growth and potential geohazard for LUSI mud volcano: East Java, Indonesia. Mar. Pet. Geol. 26, 1724–1739. http://dx.doi.org/10.1016/j.marpetgeo.2009.03.006.
Jaeger, J.C., Cook, N.G.W., Zimmerman, R.W., 2007. Fundamentals of Rock Mechanics, 4th ed. Blackwell Publishing.
Manga, M., Brumm, M., Rudolph, M.L., 2009. Earthquake triggering of mud volcanoes. Mar. Pet. Geol. 26, 1785–1798. http://dx.doi.org/10.1016/j.marpetgeo.2009.01.019.
Mazzini, A., Svensen, H., Akhmanov, G.G., Aloisi, G., Planke, S., Malthe-Sørenssen, A., Istadi, B., 2007. Triggering and dynamic evolution of the LUSI mud volcano, Indonesia. Earth Planet. Sci. Lett. 261, 375–388. http://dx.doi.org/10.1016/j.epsl.2007.07.001.
Mazzini, A., Nermoen, A., Krotkiewski, M., Podladchikov, Y., Planke, A., Svensen, H., 2009. Strike–slip faulting as a trigger mechanism for overpressure release through piercement structures. Implications for the Lusi mud volcano, Indonesia. Mar. Pet. Geol. 26, 1751–1765. http://dx.doi.org/10.1016/j.marpetgeo.2009.03.001.
Mazzini, A., Etiope, G., Svensen, H., 2012. A new hydrothermal scenario for the 2006 Lusi eruption, Indonesia. Insights from gas geochemistry. Earth Planet. Sci. Lett. 317–318, 305–318. http://dx.doi.org/10.1016/j.epsl.2011.11.016.

Menke, W., 2012. Geophysical Data Analysis: Discrete Inverse Theory, 3rd ed. Academic Press.
Murton, B.J., Biggs, J., 2003. Numerical modelling of mud volcanoes and their flows using constraints from the Gulf of Cadiz. Mar. Geol. 195, 223–236. http://dx.doi.org/10.1016/S0025-3227(02)00690-4.
Rudolph, M.L., Manga, M., 2010. Mud volcano response to the 4 April 2010 El Mayor–Cucapah earthquake. J. Geophys. Res. 115, B12211. http://dx.doi.org/10.1029/2010JB007737.
Rudolph, M.L., Karlstrom, L., Manga, M., 2011. A prediction of the longevity of the Lusi mud eruption, Indonesia. Earth Planet. Sci. Lett. 308, 124–130. http://dx.doi.org/10.1016/j.epsl.2011.05.037.
Rudolph, M.L., Shirzaei, M., Manga, M., Fukushima, Y., 2013. Evolution and future of the Lusi mud eruption inferred from ground deformation. Geophys. Res. Lett. 40, 1089–1092. http://dx.doi.org/10.1002/grl.50189.
Shimada, M., Ozawa, T., Fukushima, Y., Furuya, M., Rosenqvist, A., 2008. Japanese L-band radar improves surface deformation monitoring. EOS Trans. 89 (31), 277–278. http://dx.doi.org/10.1029/2008EO310002.
Wessel, P., Smith, W.H.F., 1998. New, improved version of generic mapping tools released. EOS Trans. 79, 579. http://dx.doi.org/10.1029/98EO00426.
Zoporowski, A., Miller, S.A., 2009. Modelling eruption cycles and decay of mud volcanoes. Mar. Pet. Geol. 26, 1879–1887. http://dx.doi.org/10.1016/j.marpetgeo.2009.03.003.